nature chemical biology

ARTICLE

PUBLISHED ONLINE: 24 OCTOBER 2016 | DOI: 10.1038/NCHEMBIO.2208

Small-molecule factor D inhibitors targeting the alternative complement pathway

Jürgen Maibaum[1]*, Sha-Mei Liao[2], Anna Vulpetti[1], Nils Ostermann[1], Stefan Randl[3], Simon Rüdisser[1], Edwige Lorthiois[1], Paul Erbel[1], Bernd Kinzel[1], Fabrice A Kolb[4], Samuel Barbieri[1], Julia Wagner[1], Corinne Durand[1], Kamal Fettis[1], Solene Dussauge[1], Nicola Hughes[1], Omar Delgado[2], Ulrich Hommel[1], Ty Gould[2], Aengus Mac Sweeney[5], Bernd Gerhartz[1], Frederic Cumin[1], Stefanie Flohr[1], Anna Schubart[1], Bruce Jaffee[2], Richard Harrison[6], Antonio Maria Risitano[7], Jörg Eder[1] & Karen Anderson[2]*

Complement is a key component of the innate immune system, recognizing pathogens and promoting their elimination. Complement component 3 (C3) is the central component of the system. Activation of C3 can be initiated by three distinct routes—the classical, the lectin and the alternative pathways—with the alternative pathway also acting as an amplification loop for the other two pathways. The protease factor D (FD) is essential for this amplification process, which, when dysregulated, predisposes individuals to diverse disorders including age-related macular degeneration and paroxysmal nocturnal hemoglobinuria (PNH). Here we describe the identification of potent and selective small-molecule inhibitors of FD. These inhibitors efficiently block alternative pathway (AP) activation and prevent both C3 deposition onto, and lysis of, PNH erythrocytes. Their oral administration inhibited lipopolysaccharide-induced AP activation in FD-humanized mice. These data demonstrate the feasibility of inhibiting the AP with small-molecule antagonists and support the development of FD inhibitors for the treatment of complement-mediated diseases.

The complement system constitutes an effective first line of defense against invading pathogens. Its components recognize pathogenic cell surfaces and trigger cell lysis and inflammatory responses[1,2]. Depending on the molecular recognition pattern, there are three distinct routes by which activation can be initiated: the classical, the lectin and the alternative pathways. These pathways converge at the proteolytic cleavage of the third component of complement, C3, generating the C3a and C3b activation fragments. C3b also participates in amplification of its own production via the positive-feedback loop of the alternative pathway (AP)[2,3]. It is subsequent to C3 activation that the major effector mechanisms of complement are expressed. These include C3-dependent opsonization, important for phagocytic elimination, and generation of the membrane-attack complex (MAC), which leads to membrane disruption and cell lysis. Dysregulation of AP activity by genetic mutations, neutralizing antibodies to complement regulatory proteins, or stabilizing antibodies to complement complexes predisposes individuals to diverse disorders including paroxysmal nocturnal hemoglobinuria (PNH), age-related macular degeneration (AMD), atypical hemolytic uremic syndrome (aHUS) and C3 glomerulonephritis (C3G)[4–7]. While disease manifestation is often local, for example, in the kidney or in the eye, many of these diseases also display systemic overactivation of the pathway, and their effective treatment may require inhibition both systemically and locally.

Complement factor D (FD) is the rate-limiting enzyme of the AP, and it plays a key role in both AP-initiated C3 activation and subsequent amplification of this central activation step. FD cleaves factor B (FB) when it is complexed with C3b to generate an active C3 convertase (C3bBb), cleaving C3 into C3a and C3b. C3b is deposited onto acceptor surfaces (opsonization). Recruitment of a further C3b molecule to the membrane-bound C3bBb complex generates a C5 convertase, leading to C5a release and MAC (C5b to C9) formation on targeted surfaces with subsequent membrane disruption and cell lysis[8]. FD is a trypsin-like S1 serine protease (228 amino acids (aa), 24 kDa), which circulates in plasma in a mature, but latent, self-inhibited form. Full proteolytic activity of FD requires a conformational change upon binding to its surface-bound endogenous substrate C3bB[9]. Latent FD is characterized by an atypical active site architecture comprising the catalytic triad in an inactive conformation, a self-inhibitory loop (aa 214–218) restricting access to the non-prime recognition sites, and an Arg218–Asp189 salt bridge at the bottom of the S1 pocket[10,11]. The protease does not recognize peptide substrates, but it still exerts weak catalytic activity against synthetic lysine-derived thioesters[12]. Irreversible covalent FD inhibitors have been reported; however, lack of specificity toward multiple other S1 proteases prevents their clinical use[13–15]. While an antigen-binding fragment (Fab) capable of neutralizing FD activity is in clinical trials for the treatment of dry age-related macular degeneration (AMD), its use is limited to intravitreal injection[16]. No specific FD inhibitors are currently available for oral therapy of diseases linked to AP dysregulation.

In this report, we describe the discovery of potent, selective and reversible small-molecule inhibitors of FD by use of a structure-based design approach in combination with fragment-based screening. These inhibitors efficiently blocked AP activation in human whole blood, and their oral administration to FD-humanized C57Bl/6 mice inhibited lipopolysaccharide (LPS)-induced AP activation both systemically and in ocular tissues. Furthermore,

[1]Novartis Institutes for BioMedical Research, Novartis Pharma AG, Novartis Campus, Basel, Switzerland. [2]Novartis Institutes for BioMedical Research, Cambridge, Massachusetts, USA. [3]Evonik Japan Co., Shinjuku-ku, Tokyo, Japan. [4]Pharma Research and Early Development, Roche Innovation Center Basel, Basel, Switzerland. [5]Drug Discovery Department, Actelion Pharmaceuticals Ltd., Allschwil, Switzerland. [6]Institute of Infection and Immunity, School of Medicine, Cardiff University, Henry Wellcome Building, Heath Park, Cardiff, UK. [7]University of Naples, Department of Clinical Medicine and Surgery, Division of Hematology, Naples, Italy. *e-mail: juergen_klaus.maibaum@novartis.com or karen.anderson@novartis.com

FD inhibition prevented C3 deposition on, and lysis of, human erythrocytes in an assay that mimics lytic sensitivity of PNH erythrocytes. These findings were confirmed with erythrocytes from PNH patients. Taken together, these data demonstrate the feasibility of inhibiting the AP with highly specific small-molecule antagonists of FD to treat complement-mediated diseases for which there are currently either no or sub-optimal therapies.

RESULTS

Identification of small-molecule factor D inhibitors

Using multiple-hit-finding strategies, we set out to discover selective small molecules, with oral bioavailability, capable of blocking FD proteolytic activity. Two high-throughput screens, based on either FD thioesterolysis or on MAC formation, failed to deliver validated hits. We therefore applied a structure-based library design approach in combination with *in silico* docking of fragments. Use of a (*S*)-proline-based library was inspired by the co-crystal structure of compound **1** in complex with kallikrein-7 (KLK7), a related S1 serine protease (**Fig. 1a**,**b**). Compound **1**, which originated from a separate drug discovery effort, occupies the buried S1 pocket and extends into the prime site (S1′–S2′) with the catalytic His57 side chain in a displaced non-catalytic conformation. The orientation of KLK7-bound **1**, forming several key hydrogen bond interactions, suggested that this binding pose might be compatible with the topology of the latent FD active site[10], thus providing us with an attractive opportunity for a FD-tailored inhibitor design.

A set of proline analogs of **1**, bearing moieties that could reach into the S1 and S2′ pockets, was selected for synthesis based on docking (GLIDE[17]) of a virtual library to the crystal structure of FD (**Supplementary Results**, **Supplementary Fig. 1a**,**b**). Evaluation of these compounds for inhibition of FD proteolytic activity against a thioester-based substrate identified compound **2** (**Fig. 1a**), which showed a half-maximum inhibitory concentration (IC_{50}) of 14 μM (**Supplementary Table 1**) and was equipotent against KLK7 (IC_{50} = 9 μM). ^{1}H–^{15}N HSQC NMR spectroscopy[18] was used to demonstrate direct binding of **2** to uniformly ^{15}N-labeled FD (**Supplementary Fig. 1c**). We further developed an *in vitro* FD proteolytic assay to determine the inhibition of the formation of the factor B cleavage product Ba (**Supplementary Fig. 2**) using the cobra venom factor (CVF)–FB complex as a surrogate endogenous substrate[19]. Consistent with the biochemical and biophysical data, **2** inhibited FD proteolytic activity against the CVF–FB complex with an IC_{50} value of 33 μM, confirming **2** as a viable starting point for further optimization.

The crystal structure of **2** in complex with FD (**Fig. 1c**) revealed key binding features consistent with our library design concept. The molecule binds in a bent conformation, penetrating deeply into the S1 pocket and occupying the S1′ and S2′ sites. The benzoate moiety is flanked by Gly216–Arg218 of the self-inhibitory loop and packs against the Cys191–Lys192 peptide bond, positioning the carboxylic ester oxygen at a 3.4-Å distance to the nitrogen of Arg218 at the bottom of the S1 pocket. The urea spacer carbonyl is within binding distance to the NH of Gly193 forming part of the oxyanion hole. The His57 side chain adopts an outward conformation to accommodate the central proline scaffold in close proximity to the Cys42–Cys58 disulfide bond, and the CF_3O group of **2** is positioned in a small hydrophobic indentation of the S2′ binding site.

Generation of potent and selective inhibitors

To discover alternative S1 binding structural motifs with improved affinity and on-target selectivity, we employed fragment-based screening[20]. Fragments are molecules of low molecular weight, typically well below 300 Da, and high solubility, rendering them suitable to bind to cryptic or transient pockets of protein surfaces. Because of their intrinsically lower complexity, they are much better suited than larger-sized ligands to sample the chemical space of a binding

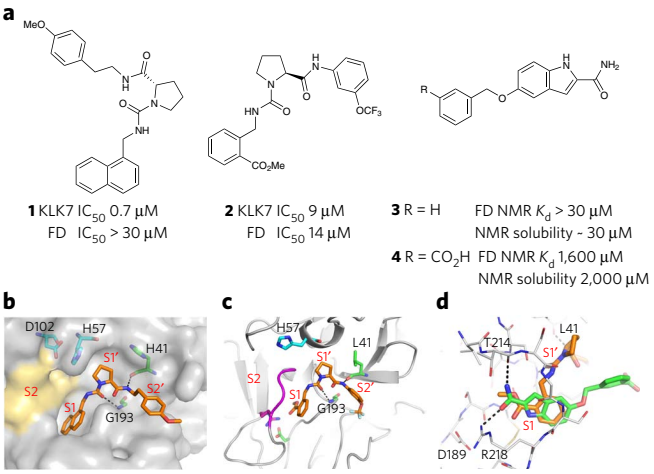

Figure 1 | Structure-based evolution of reversible small-molecule human FD inhibitors. (**a**) Structure, binding affinities and *in vitro* potencies of compounds **1**–**4** determined by protein NMR and biochemical assays. (**b**) Co-crystal structure of **1** (orange) in complex with KLK7. Hydrogen bonds to Gly193 and His41 are highlighted. The surface of the unoccupied S2 site is colored in yellow. (**c**) Ribbon diagram of the FD active site in complex with **2** (orange) spanning S1–S2′. The self-inhibitory loop (pink) is in a closed, the His57 side chain in a non-catalytic 'outward' conformation. (**d**) Superposition of **2** (orange) and **4** (green) showing hydrogen bonds of the **4** carboxamide to Arg218/Thr214. The **4** benzoate moiety is exposed to solvent.

site[21]. Consequently, hits are generally more frequent in fragment-based screening than in HTS campaigns, but they may bind only weakly to the biological target. This necessitates growing or combining fragments with other structural motifs, such as compound **2** in the case of FD, in order to generate compounds with higher affinity. Rather than screening random libraries of fragments, we chose a focused, structure-based approach and first selected a set of 52,000 fragments (molecular weight ≤ 350 Da; **Supplementary Fig. 3a**), docking them *in silico* into distinct FD active site conformations based on the PDB 1DIC[14] crystal structure. Screening of a diverse set of top-scoring fragments at 100 μM (nominal concentration) by ligand-observation NMR (WaterLOGSY[22]) in the presence of FD identified **3** (**Fig. 1a**) as a hit. To ascertain binding and allow for quantification of binding affinity, we synthesized a more water-soluble carboxylic acid analog, **4** (**Fig. 1a**), which, in contrast to **3**, showed concentration-dependent chemical shift changes in the ^{1}H–^{15}N HSQC NMR spectrum (average NMR dissociation constant (K_d) = 1,600 μM; **Supplementary Fig. 3b**,**c**). The co-crystal structure of **4** bound to FD (1.46-Å resolution) showed the 2-carboxamide indole positioned in S1 and flanked by the self-inhibitory loop and the Lys192 side chain (**Fig. 1d**). The deeply buried terminal carboxamide group is hydrogen bonded to the Arg218 guanidine and the Thr214 carbonyl of the S1 pocket, and the tethered benzoic acid moiety of **4** is exposed to the solvent space without making direct binding contacts to the protein.

The co-planar superposition of the S1 binding moiety of **4** with the *ortho*-benzoic ester portion of **2** (**Fig. 1d**) prompted us to merge both inhibitors. The design concept was supported by proline analog **5** (IC_{50} = 5.8 μM, thioesterolysis assay; **Fig. 2a**), which was identified by a retrospective structure-similarity search in the Novartis compound collection and was predicted by computational modeling to bind with its *N*-methylindole portion to S1 in a similar overlapping pose (**Fig. 2b**). Combining a carboxamide group, as in **4**, with an indole-like scaffold, as in **5**, followed by further extensive chemical optimization in a number of iterative design cycles, led to the 6-aza-indazole **6** (**Fig. 2a**) as a highly potent and selective

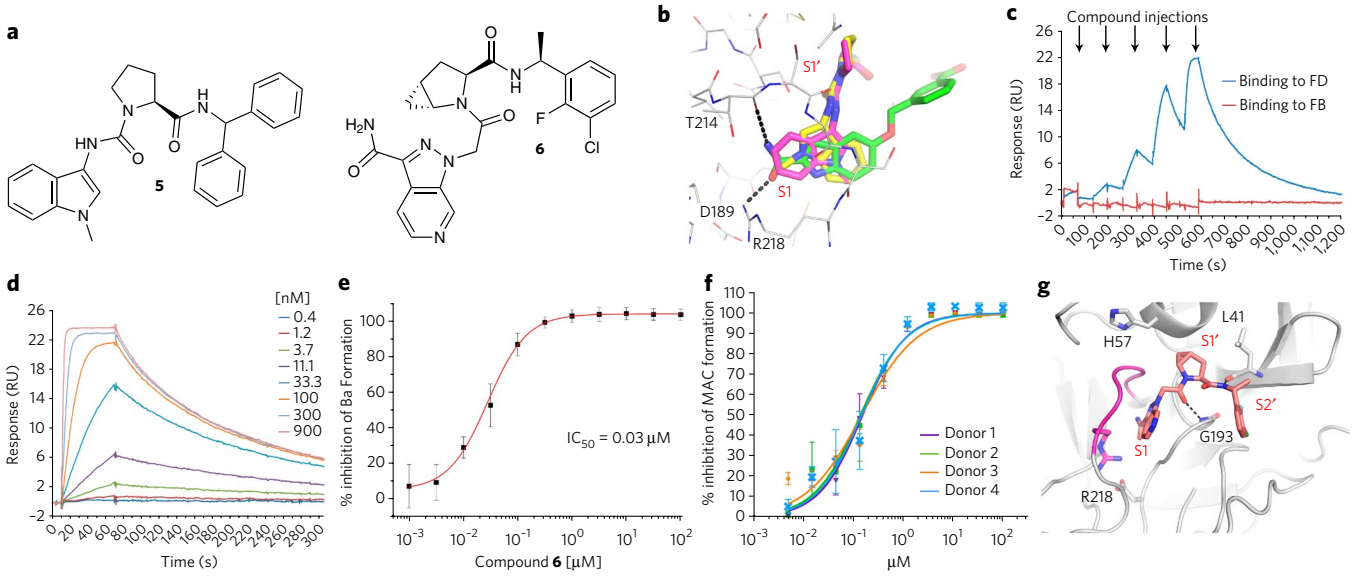

Figure 2 | Identification and characterization of potent and selective human FD inhibitor 6. (**a**) Chemical structures of **5** and **6**. (**b**) Computational model of **5** (yellow and pink sticks) in complex with FD suggesting two distinct binding conformations of the indole portion within the S1 pocket. Overlaid is the crystal structure of **4** (green sticks) in complex with FD. (**c**) Direct binding of **6** to immobilized FD (blue) and FB (red) determined by SPR spectroscopy. Proteins were exposed (arrows) to increasing concentrations of **6** (single-cycle kinetics). RU, response units. (**d**) Binding of **6** to immobilized FD by standard kinetics SPR. (**e**) IC_{50} determination (n = 4 experiments) for inhibition of FD activity by **6** as indicated by formation of the FB cleavage product Ba, using CVF–FB as substrate. (**f**) Inhibition of AP-mediated MAC formation by **6** in 50% whole blood from four individual donors. Error bars denote s.d. of three technical replicates. Average IC_{50} value was 144 nM. (**g**) Crystal structure of FD-bound **6** spanning the S1–S2′ pockets. Self-inhibitory loop (pink) is in closed conformation and His57 in 'outward' position.

inhibitor of FD. In a direct binding assay using surface plasmon resonance (SPR) spectroscopy, **6** showed an average K_d of 0.006 µM (**Fig. 2c,d**; **Supplementary Table 2**), with a fast association of the protein–ligand complex (k_{on} = 1.64 × 10^6 $M^{-1}s^{-1}$), and did not show binding to factor B, the second serine protease of the alternative pathway. Proteolytic cleavage of FB by FD in the biochemical assay was inhibited by **6** with an IC_{50} value of 0.03 µM (**Fig. 2e**).

Next we determined the ability of compound **6** to inhibit AP activation in a more physiological setting. The inhibitor effectively blocked both AP-mediated hemolysis in 10% human serum (IC_{50} = 0.006 µM) and AP-induced MAC formation in lepirudin-anticoagulated 50% human whole blood (IC_{50} = 0.14 µM; **Fig. 2f**). Moreover, **6** is highly selective for human FD, showing no inhibition of FB proteolytic activity (**Supplementary Fig. 2c,d**), no inhibition of classical and lectin complement-pathway activation (see Online Methods), and no significant effects (up to 10 µM) in a broad assay panel of receptors, ion channels, kinases and proteases (**Supplementary Table 1**).

The crystal structure of **6** bound to FD confirmed the overall binding pose extending from S1 to S2′, with the self-inhibitory loop shielding the non-prime site and the catalytic His57 adopting a 'non-canonical' catalytic-triad conformation (**Fig. 2g**). The terminal carboxamide group of the ligand is in close binding contact to Arg218 and forms additional water-mediated hydrogen bonds with Ser190 and Ile227 in S1 and the backbone NH of Gly193 and the carbonyl of Leu41. The *meta*-Cl substituent positioned in S2′ forms a halogen–carbonyl bond with Trp141; the *ortho*-F atom further strengthens this interaction.

Compound 6 selectively blocks factor D activity *in vivo*

Compound **6** demonstrated only modest inhibition of murine FD (IC_{50} = 0.86 µM). In order to understand the striking difference in human versus mouse IC_{50} values, we solved the crystal structure of murine FD at 1.25-Å resolution, which revealed that the self-inhibitory loop (Trp215–Arg218) adopts a distinct conformation compared to the human protease[23], with the carbonyl group of Gly216 preventing inhibitor binding to the narrower S1 pocket. A significant conformational movement of the murine FD self-inhibitory loop would thus be required in order to accommodate inhibitor **6** in the S1 binding site (**Fig. 3a**).

In order to pursue *in vivo* pharmacology studies, we generated C57Bl/6 mice expressing only the human orthologous enzyme (human-FD knock-in (KI) mice) (**Fig. 3b**). The average human-FD blood level of female KI mice used for *in vivo* studies was 0.78 µg/mL (**Fig. 3c**) and hence within the range reported for humans[24]. Reconstitution experiments with serum obtained from *CFD*$^{-/-}$ mice demonstrated that human FD effectively activates murine FB, as previously reported[25]. In line with the species selectivity seen for inhibition of FD, which is a result of the different active site architectures, compound **6** blocked C3 cleavage only in the serum of mice expressing human FD, but not in serum of wild-type mice (**Fig. 3d**). These results provide strong experimental evidence that the inhibition of the alternative complement pathway in the presence of compound **6** is indeed target specific.

AMD patients commonly have genetic alterations in AP components and evidence of systemic AP overactivity[24,26–28] with pathology that manifests in retinal tissue. We sought to model systemic complement activation in mice by injection of lipopolysaccharide (LPS). In human-FD KI mice we observed a dose- and time-dependent increase in AP activation after intraperitoneal (i.p.) injection of LPS, as indicated by rising levels of Ba and the C3 breakdown products C3d and iC3b in both plasma and ocular tissue (**Supplementary Fig. 4**). At the 7.5-h time point after LPS administration, levels of Ba or C3d/iC3b were ~2- to 3-fold of those in the control group. When administered by oral gavage 3.5 h after LPS, compound **6** dose-dependently inhibited complement activation as determined 4 h post-dose in both plasma and ocular tissue, with full inhibition at 10 mg/kg (**Fig. 4a,b**). Technical limitations do not allow clean separation of retinal tissue from the eye vasculature, limiting the conclusions that can be drawn with respect to local retinal complement

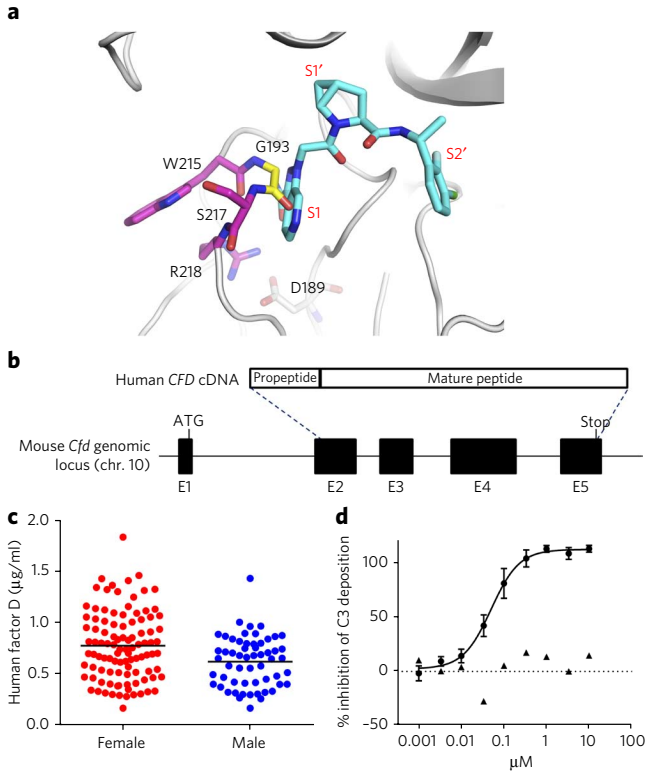

Figure 3 | Generation of human factor D knock-in mice. (**a**) Ribbon diagram of apo-mouse FD active site. Trp215, Gly216, Ser217 and Arg218 of the self-inhibitory loop are highlighted as sticks (pink color, with Gly216 in yellow). Overlaid is the structure of **6** (turquoise sticks) in its binding pose in complex with human FD (protein structure omitted). (**b**) Schematic representation of the mouse *Cfd* gene locus (bottom). The five exons are displayed as black boxes (E1–E5), and the ATG start codon as well as the stop codon are indicated. The human *CFD* cDNA encoding for the propeptide and the mature FD protein are shown on top. Integration sites of the human *CFD* cDNA in the mouse *Cfd* gene are indicated as dashed lines. Insertion of the human cDNA leads to partial replacements of mouse exons 2 and 5 and to complete deletion of mouse exons 3 and 4. (**c**) Human FD levels in the blood of female (n = 101) and male (n = 57) C57Bl/6 human-FD knock-in (hFD KI) mice were quantitated by western blotting with anti-human FD antibody. Average plasma levels ± s.d. were 0.78 ± 0.33 μg/mL and 0.63 ± 0.24 μg/mL, respectively. (**d**) Compound **6** inhibits C3 deposition in 50% serum of hFD KI mice (circles; IC_{50} value of 0.07 ± 0.03 μM, n = 4, mean ± s.d.), but not wild-type mice (triangles; n = 2).

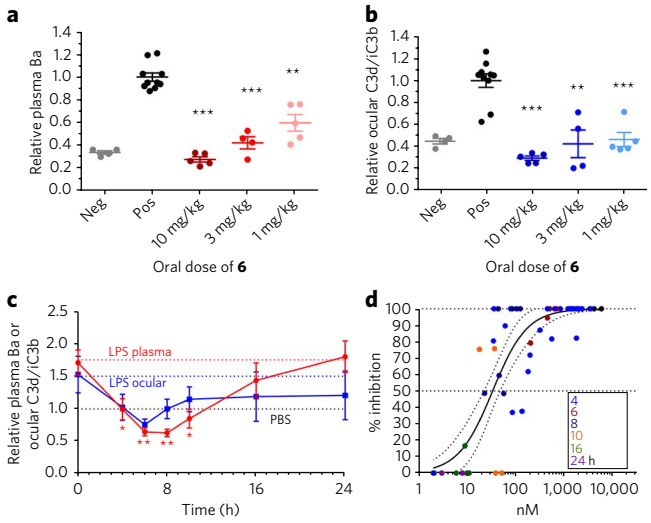

Figure 4 | Inhibitor (6) blocks LPS-induced systemic and ocular AP activation in C57Bl/6 mice expressing human FD. (**a**,**b**) Dose-dependent inhibition of plasma Ba (**a**) and ocular C3d/iC3b (**b**) determined 4 h after oral dosing of **6** (1, 3, and 10 mg/kg) given 3.5 h after LPS injection. Negative (Neg) and positive control group (Pos) are indicated (see Online Methods and **Supplementary Fig. 5**). n = 4–10 female mice per group as indicated. (**c**) Plasma Ba and ocular C3d/iC3b levels after one 30 mg/kg dose of **6**, administered to separate groups of mice 24, 16, 10, 8, 6, or 4 h before tissue collection (see Online Methods and **Supplementary Fig. 5**). The level of breakdown products in Neg was set at 1 (line labeled PBS); the level in Pos is indicated by the lines labeled LPS. n = 4 mice per group. Data shown as mean ± s.e.m. in **a**–**c**; $^*P < 0.05$, $^{**}P < 0.01$, $^{***}P < 0.001$ compared to positive control in **a**–**c** by ANOVA with Dunnett's post test. (**d**) Terminal concentration of **6** in each sample from dose–response and duration-of-action studies (n = 62), relative to plasma Ba inhibition, was used to calculate EC_{50} = 0.034 μM for **6**. Dashed lines represent the 95% confidence band. Data points on graph are color coded to time (h) after compound administration.

inhibition and blood-retina barrier penetration of **6** in mice. To test the duration of action, a single 30 mg/kg oral dose of **6** was given to separate groups of mice at time points ranging from 4 to 24 h before study termination, while LPS (i.p.) was given 7.5 h before termination in all animals to maintain a consistent interval of LPS exposure (**Supplementary Fig. 5**). Compound **6** showed sustained inhibition of LPS-induced AP activation for at least 8 h post-dose with a half-maximal efficacious concentration (EC_{50}) of 0.034 μM (**Fig. 4c**,**d**).

Factor D inhibition prevents lysis of PNH erythrocytes

Importantly, compound **6** was active in an assay that mimics complement deposition onto, and hemolysis of, PNH erythrocytes (**Fig. 5a** and **Supplementary Fig. 6**). PNH is caused by a somatic mutation in the *PIGA* gene in hematopoietic stem cells, resulting in deficiency of glycosylphosphatidylinositol (GPI)-anchored complement regulators CD55 and CD59 (ref. 5). To simulate the pathophysiology *in vitro*, normal human red blood cells (RBCs) were incubated with blocking antibodies against CD55 and CD59, and the AP was activated by serum acidification[29]. Compound **6** inhibited both hemolysis and C3 deposition on the surface of RBCs with an IC_{50} value of 0.07 μM, consistent with inhibition of the AP amplification loop. In contrast, the anti-C5 monoclonal antibody eculizumab, the current standard of care for PNH[30], blocked hemolysis but generated erythrocytes that were extensively coated with C3 fragments (**Fig. 5a** and **Supplementary Fig. 6**). Such C3-fragment-coated RBCs are commonly observed in eculizumab-treated PNH patients[31] and are susceptible to extravascular hemolysis in the spleen and liver. This C3 coating provides a plausible explanation for the finding that ~40% of eculizumab-treated patients remain transfusion dependent[29]. Furthermore, using erythrocytes from PNH patients, we examined the *ex vivo* efficacy of the structurally related compound **7** (**Fig. 5b**), which has similar *in vitro* potency to compound **6** (**Supplementary Table 1**; IC_{50} = 0.05 μM in the AP-induced MAC formation assay using 50% human whole blood), but showed higher permeability and no efflux in Caco-2 cells[32] (P_{app} (A-B) × 10^{-6} (cm/s) = 15.3; P_{app} (B-A) × 10^{-6} (cm/s) = 18.1; (B-A)/(A-B) = 1.19; respective values for compound **6**: 1.35, 9.66 and 7.17) and improved oral bioavailability (F = 100%) in rat (**Supplementary Table 4**; for compound **6**: F = 28%). In line with its activity in the surrogate PNH assay, compound **7** fully blocked C3 deposition on the surface of CD59-negative PNH erythrocytes and prevented their lysis (**Fig. 5a**,**c**,**d**). Targeting the AP amplification loop in PNH therefore has the potential advantage over anti-C5 therapy of blocking not only extravascular hemolysis, but also any C3-driven pathology.

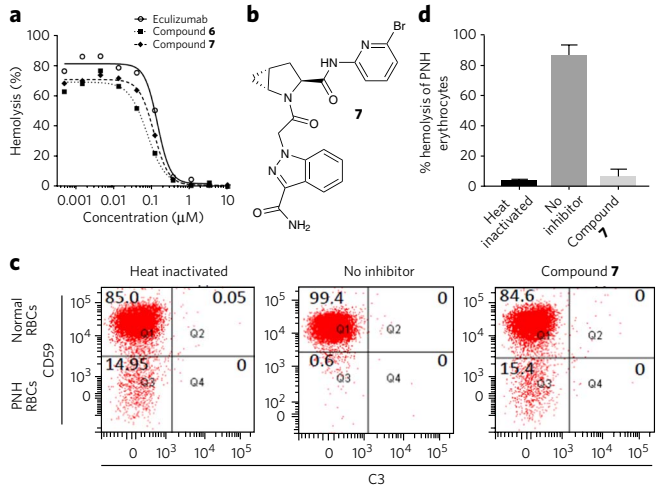

Figure 5 | Inhibitors of FD prevent C3 deposition on and hemolysis of PNH erythrocytes. (**a**) Dose–response curves for inhibition of hemolysis of erythrocytes from healthy donors for compound **6**, compound **7**, and eculizumab (see Online Methods and **Supplementary Fig. 6**). Erythrocytes were incubated with CD55/CD59 blocking antibodies and transferred into acidified serum in the presence of Mg^{2+}–EGTA to limit activation to the alternative pathway and prevent antibody-mediated activation of the classical pathway. Hemolysis was measured by increase in optical density. Curves are representatives of $n = 11$ (compound **6**), $n = 2$ (compound **7**) and $n = 7$ (eculizumab) measurements. (**b**) Structure of compound **7**. (**c**) Compound **7** (1 μM) blocks hemolysis of CD59-negative erythrocytes from a PNH patient. C3 deposition was assessed using a C3 polyclonal antibody. Number of RBCs in each quadrant is indicated. Heat inactivation neutralizes serum complement activity. Note that lysed CD59-negative PNH erythrocytes disappear from the gate in the absence of inhibitor, and no C3 deposition could be detected. (**d**) Inhibition of hemolysis of PNH erythrocytes. Blood from 3 patients was analyzed in 2–14 repeats; mean ± s.e.m. is shown. Compound **7** was used at 1 μM. Hemolysis of PNH erythrocytes was determined by flow cytometry (see Online Methods).

DISCUSSION

The non-canonical active site architecture of latent factor D, characterized by a distorted conformation of the catalytic triad and a self-inhibitory loop that prevents access to the non-prime sites, renders this enzyme of the S1 protease family a challenging target for drug discovery. This is reflected by the fact that we did not find any suitable inhibitor by high-throughput screening of a 1.2 million compound collection. The work described here demonstrates the utility of structure-based focused screening and rational drug design coupled with a chemical library approach to discover potent, selective and reversible small-molecule inhibitors of FD. Central to the optimization of the initial inhibitors was the subsequent dedicated screening of an *in silico*–selected target-focused fragment library, which, in combination with a detailed structural understanding of the binding modes of the various compounds, allowed the combination of different structural motifs and ultimately led to the final inhibitors. Although an Fab fragment capable of neutralizing FD catalytic activity is currently in clinical trials for the treatment of geographic atrophy, its use is restricted to local injection. In addition to the inherent short half-life of Fab fragments, the steady-state level of endogenous FD, the result of a high production rate coupled with rapid renal clearance, is unfavorably disturbed by systemic application of a FD antibody or antibody fragment[16]. Therefore, our small-molecule compounds are the first inhibitors that would allow sustained inhibition of FD at a systemic level.

Significant species specificity for human versus mouse FD was observed for this inhibitor chemotype. This can be rationalized by the distinct active site conformations of murine and human FD as revealed by X-ray crystallography. Consequently, compound **6** did not block AP activation in the serum of wild-type C57Bl/6 mice, and we had to generate human-FD KI mice to demonstrate AP inhibition *in vivo*. Based on these findings, as well as on the compound's favorable biochemical profile in terms of potency and selectivity, we conclude that the *in vivo* and *ex vivo* effects observed with our inhibitors are in fact the result of selectively blocking FD proteolytic activity.

Inhibitors **6** and **7** were active in an assay that mimics PNH pathophysiology. Both compounds not only blocked AP-induced hemolysis but also inhibited C3 opsonization of erythrocytes. Additionally, compound **7** was found to prevent both lysis and opsonization of erythrocytes from PNH patients. Opsonizing C3 fragments are recognized by complement receptors 1, 3 and 4 expressed on phagocytes and Kupffer cells, rendering C3-coated erythrocytes subject to destruction by extravascular hemolysis in the liver and spleen. Extravascular hemolysis often becomes more apparent in patients receiving anti-C5 therapy, which prevents MAC-mediated intravascular lysis but does not block C3 deposition on erythrocytes[31]. Inhibition of FD may therefore offer a therapeutic advantage over the current standard of care in PNH treatment. In addition, systemic dysregulation of the AP consequent to genetic mutations in its constituent proteins, or auto-antibodies stabilizing the C3 convertase (either directly or by neutralization of complement regulatory proteins), predisposes to a number of diseases with local manifestation in organs such as the kidney. Fully effective treatment of these diseases may require AP inhibition at a systemic level, and our findings support the potential clinical utility of oral FD inhibitors for such use.

Genetic deficiency of AP components is associated with increased susceptibility to bacterial infection[33]. It will therefore be important to evaluate the clinical safety of FD inhibitors, not just for on-target and off-target risks traditionally associated with drug discovery, but also for infection risk. In this context it is possible that specific alternative-pathway blockade, when compared to C5 blockade, may carry a reduced risk for infections such as *Neisseria meningitidis*, for which the lytic pathway is critically important for bacterial elimination. This will be particularly true if patients are adequately vaccinated and can therefore recruit the lytic pathway through efficient antibody-dependent classical pathway activation. In addition, the use of small-molecule inhibitors would, in principle, allow more tunable pharmacologic intervention than that with antibody-based therapies. This may be important for diseases where AP activation is the result of an imbalance between stimulatory and regulatory mechanisms, for example, due to genetic polymorphisms (AMD) or somatic mutations (PNH), where the therapeutic objective would be to convert the patient's status from high-risk to low-risk phenotype. If feasible, this would permit better titration for the desired therapeutic effect versus any potential side effects.

The work presented here offers a new way to target the alternative pathway in the treatment of complement-related diseases. The next logical step in their development will be to define the clinical safety profile of FD inhibitors, and to evaluate this, on an indication-specific basis, against the exciting prospect for their significant therapeutic benefit.

Received 20 May 2016; accepted 15 August 2016;
published online 24 October 2016

METHODS

Methods and any associated references are available in the online version of the paper.

Accession codes. Atomic coordinates and structure factors for the human KLK7–**1** complex, for human FD in complex with compounds **2**, **4** and **6**, and for the mouse apo-FD are deposited in the Protein Data Bank with accession codes 5FAH, 5FBE, 5FBI, 5FCK and 5FCR, respectively.

References

1. Walport, M.J. Complement. Second of two parts. *N. Engl. J. Med.* **344**, 1140–1144 (2001).
2. Ricklin, D., Hajishengallis, G., Yang, K. & Lambris, J.D. Complement: a key system for immune surveillance and homeostasis. *Nat. Immunol.* **11**, 785–797 (2010).
3. Thurman, J.M. & Holers, V.M. The central role of the alternative complement pathway in human disease. *J. Immunol.* **176**, 1305–1310 (2006).
4. Holers, V.M. The spectrum of complement alternative pathway-mediated diseases. *Immunol. Rev.* **223**, 300–316 (2008).
5. Risitano, A.M. Paroxysmal nocturnal hemoglobinuria and the complement system: recent insights and novel anticomplement strategies. *Adv. Exp. Med. Biol.* **735**, 155–172 (2013).
6. Zipfel, P.F. *et al.* The role of complement in C3 glomerulopathy. *Mol. Immunol.* **67**, 21–30 (2015).
7. Zipfel, P.F., Heinen, S., Józsi, M. & Skerka, C. Complement and diseases: defective alternative pathway control results in kidney and eye diseases. *Mol. Immunol.* **43**, 97–106 (2006).
8. Lesavre, P.H. & Müller-Eberhard, H.J. Mechanism of action of factor D of the alternative complement pathway. *J. Exp. Med.* **148**, 1498–1509 (1978).
9. Forneris, F. *et al.* Structures of C3b in complex with factors B and D give insight into complement convertase formation. *Science* **330**, 1816–1820 (2010).
10. Volanakis, J.E. & Narayana, S.V.L. Complement factor D, a novel serine protease. *Protein Sci.* **5**, 553–564 (1996).
11. Schechter, I. & Berger, A. On the size of the active site in proteases. I. Papain. *Biochem. Biophys. Res. Commun.* **27**, 157–162 (1967).
12. Kam, C.M. *et al.* Human complement proteins D, C2, and B. Active site mapping with peptide thioester substrates. *J. Biol. Chem.* **262**, 3444–3451 (1987).
13. Ikari, N., Sakai, Y., Hitomi, Y. & Fujii, S. New synthetic inhibitor to the alternative complement pathway. *Immunology* **49**, 685–691 (1983).
14. Cole, L.B., Kilpatrick, J.M., Chu, N. & Babu, Y.S. Structure of 3,4-dichloroisocoumarin-inhibited factor D. *Acta Crystallogr. D Biol. Crystallogr.* **54**, 711–717 (1998).
15. Morikis, D. & Lambris, J.D. Structural aspects and design of low-molecular-mass complement inhibitors. *Biochem. Soc. Trans.* **30**, 1026–1036 (2002).
16. Loyet, K.M. *et al.* Complement inhibition in cynomolgus monkeys by anti-factor d antigen-binding fragment for the treatment of an advanced form of dry age-related macular degeneration. *J. Pharmacol. Exp. Ther.* **351**, 527–537 (2014).
17. Halgren, T.A. *et al.* Glide: a new approach for rapid, accurate docking and scoring. 2. Enrichment factors in database screening. *J. Med. Chem.* **47**, 1750–1759 (2004).
18. Bodenhausen, G. & Ruben, D.J. Natural abundance nitrogen-15 NMR by enhanced heteronuclear spectroscopy. *Chem. Phys. Lett.* **69**, 185–189 (1980).
19. Pangburn, M.K. & Müller-Eberhard, H.J. The C3 convertase of the alternative pathway of human complement. Enzymic properties of the bimolecular proteinase. *Biochem. J.* **235**, 723–730 (1986).
20. Murray, C.W. & Blundell, T.L. Structural biology in fragment-based drug design. *Curr. Opin. Struct. Biol.* **20**, 497–507 (2010).
21. Hann, M.M., Leach, A.R. & Harper, G. Molecular complexity and its impact on the probability of finding leads for drug discovery. *J. Chem. Inf. Comput. Sci.* **41**, 856–864 (2001).
22. Dalvit, C. *et al.* Identification of compounds with binding affinity to proteins via magnetization transfer from bulk water. *J. Biomol. NMR* **18**, 65–68 (2000).
23. Min, H.Y. & Spiegelman, B.M. Adipsin, the adipocyte serine protease: gene structure and control of expression by tumor necrosis factor. *Nucleic Acids Res.* **14**, 8879–8892 (1986).
24. Scholl, H.P. *et al.* Systemic complement activation in age-related macular degeneration. *PLoS One* **3**, e2593 (2008).
25. Xu, Y. *et al.* Complement activation in factor D-deficient mice. *Proc. Natl. Acad. Sci. USA* **98**, 14577–14582 (2001).
26. Reynolds, R. *et al.* Plasma complement components and activation fragments: associations with age-related macular degeneration genotypes and phenotypes. *Invest. Ophthalmol. Vis. Sci.* **50**, 5818–5827 (2009).
27. Hecker, L.A. *et al.* Genetic control of the alternative pathway of complement in humans and age-related macular degeneration. *Hum. Mol. Genet.* **19**, 209–215 (2010).
28. Ristau, T. *et al.* Impact of the common genetic associations of age-related macular degeneration upon systemic complement component C3d levels. *PLoS One* **9**, e93459 (2014).
29. Fishelson, Z., Horstmann, R.D. & Müller-Eberhard, H.J. Regulation of the alternative pathway of complement by pH. *J. Immunol.* **138**, 3392–3395 (1987).
30. Hillmen, P. *et al.* Long-term safety and efficacy of sustained eculizumab treatment in patients with paroxysmal nocturnal haemoglobinuria. *Br. J. Haematol.* **162**, 62–73 (2013).
31. Risitano, A.M. *et al.* Complement fraction 3 binding on erythrocytes as additional mechanism of disease in paroxysmal nocturnal hemoglobinuria patients treated by eculizumab. *Blood* **113**, 4094–4100 (2009).
32. Skolnik, S. *et al.* Towards prediction of in vivo intestinal absorption using a 96-well Caco-2 assay. *J. Pharm. Sci.* **99**, 3246–3265 (2010).
33. Ram, S., Lewis, L.A. & Rice, P.A. Infections of people with complement deficiencies and patients who have undergone splenectomy. *Clin. Microbiol. Rev.* **23**, 740–780 (2010).

Acknowledgments

We thank T. Zoller for the preparation of the proline-based compound library, J. Wirsching, T. Doll and A. Isken for their assistance in generating the human FD knock-in mice, N. Buchanan for coordinating the maintenance of the mouse colony, F. Zink for assistance in preparing FD and KLK7 inhibitor complex crystals, S. Kapps for preparation of ^{15}N-labeled human FD, C. Towler for small molecule crystallization experiments, C. Dentel and F. Tritsch for chemical syntheses, U. Argikar, A. Brown, S. Bailey and G. Marsh for pharmacokinetic and bioanalytical support, A. De Erkenez for performing human whole blood assays, and L. Ferrara for performing the AP hemolytic assay.

Author Contributions

N.O. and A.M.S. solved the structures by X-ray crystallography. S. Randl, U.H., A.V., E.L. and J.M. designed the FD structure-based inhibitors. S.D., C.D. and K.F. synthesized compounds. S. Rüdisser and P.E. performed NMR experiments for screening and binding affinity measurements. N.H. and P.E. conducted SPR experiments. F.C. generated the biochemical assay data. A.S. and J.W. performed the PNH surrogate assay and analyzed the data. A.M.R. performed the assays using erthrocytes from PNH patient and analyzed the data. S.B., B.K. and F.A.K. generated the human FD knock-in mice. B.G. and J.E. produced recombinant proteins. T.G. designed and interpreted pharmacokinetic studies. O.D. and S.-M.L. performed the *in vivo* studies in mice. S.F. and B.J. conceived experiments and supervised part of the work. J.M., J.E., A.S., R.H. and K.A. conceived experiments, supervised the work, and wrote the manuscript.

Competing financial interests

The authors declare competing financial interests: details accompany the online version of the paper.

Additional information

Any supplementary information, chemical compound information and source data are available in the online version of the paper. Reprints and permissions information is available online at http://www.nature.com/reprints/index.html. Correspondence and requests for materials should be addressed to J.M. or K.A.

ONLINE METHODS

Materials. Cobra venom factor (CVF) was purchased from Quidel. Anti-Ba neoepitope IgGs have been raised in rabbit and were purified from serum (Eurogentec). Anti-C3a neoepitope antibodies were purchased from Hycult. The thiol-scavenging reagent 2,4-dinitrobenzenesulfonyl-2,7-desmethyl-fluorecein was prepared according to the published protocol[34]. Anti C9 neoepitope antibody (clone aE11) conjugated to alkaline phosphatase for detection of MAC deposition was custom ordered from Diatec Monoclonals AS. Zymosan A was obtained from Sigma (Z-4250). Anti-mouse C3b/iC3b/C3c (Hycult biotech; HM1065) was obtained from Hycult Biotech and Goat anti-rat IgG HRP-conjugated Antibody from Southern Biotech (3010-05). Anti-CD55 clone HD1A (mIgG2b) was kindly provided by P. Morgan, University of Cardiff, UK[35]. Anti-CD59 clone MEM43 (mIgG2a) was purchased from ABCAM, anti-C3d (neo) mIgG1 from Quidel (A250) and anti-C5b-9 (C9 neoepitope, clone aE11; mIgG2a) from Life Technologies. Antibodies were pre-labeled using Zenon Alexa Fluor 488 mouse IgG1 or Zenon Alexa Fluor 647 mouse IgG2a Labeling Kit obtained from Life Technologies. FITC-conjugated anti-C3 polyclonal antibody was obtained from Abcam (Ab14396) and PE-conjugated anti-CD59 monoclonal antibody from Valter Occhiena (59-PE). The anti-C5 monoclonal antibody eculizumab (Soliris) was obtained from a US Pharmacy. All other chemicals were of analytical grade. For western blot detection of mouse Ba and C3d+iC3b, a polyclonal anti-human factor B (Quidel, A311) and polyclonal anti-mouse C3d (R&D Systems; AF2655) were used. Human factor D was detected using goat polyclonal anti-human antibody (R&D Systems; AF1824).

Preparation of recombinant murine and human FD catalytic domains. Mouse *Cfd* (UniProt; P03953) catalytic domain (G24–T253) was amplified by RT-PCR from C57Bl/6 RNA (lung), whereas human *CFD* (UniProt; P00746) catalytic domain (G24-A253) was amplified by PCR using an in-house cDNA collection. The PCR products were cloned into pET24 (Novagen) and expressed in *Escherichia coli* (Rosetta) in the form of inclusion bodies. Inclusion bodies were solubilized in 6 M guadinium HCl containing 100 mM DTT to reach a protein concentration of approximately 5 to 10 mg/mL. Pro-FD refolding was obtained by rapid dilution of solubilized inclusion bodies at 10 °C with 50 mM Tris/HCl (pH 8.5) containing 0.8 M arginine, 10 mM $CaCl_2$, 1 mM EDTA, 1 mM GSH, and 0.5 mM glutathione disulfide (GSSG), leading to a final protein concentration of 50 µg/mL. After gentle agitation at 10 °C for one day, the protein was concentrated and purified by size-exclusion chromatography (SEC). FD catalytic domain was formed by removal of the pro-petide sequence in the presence of trypsin-coated beads for 6 h at 8 °C. For the analogous preparation of uniformly ^{15}N-isotope-labeled human FD, an M9 minimal medium with [^{15}N] H_4Cl as the sole nitrogen source was used.

Preparation of recombinant human complement FB. The catalytic domain (Asp470–Leu764) of human *CFB* (UniProt; P00751) was amplified by PCR using an in-house cDNA collection. The PCR product was cloned into pMT–BIP and expressed in *Drosophila* SL3 cells that were grown in Sf-900 II medium containing 1% FCS (Invitrogen) as stable cell-line pools. Catalytic domain FB protein was purified from the cell culture medium by ultrafiltration and SEC.

Preparation of recombinant human KLK7 (Y180R mutant). Human *KLK7* (aa 37–253) (UniProt; P49862) was amplified by PCR using an in-house cDNA collection. To prevent autocleavage of KLK7, residue Tyr180 was replaced by Arg. The PCR products were cloned into a modified pET-24 vector (Novagen) directly after the N-terminal extension comprising His-tag, pro-peptide and enterokinase cleavage site. KLK7 was expressed in *Escherichia coli* BL21(DE3) in the form of inclusion bodies and was refolded by rapid dilution of solubilized inclusion bodies at 10 °C with 50 mM Tris/HCl pH 8.0 buffer (10 °C cold) containing 2 M urea, 500 mM NaCl, 10 mM $CaCl_2$, 0.1 M NH_4Cl, 1 mM EDTA, 1.25 mM GSH and 0.5 mM GSSG at a final protein concentration of 50 µg/mL. Refolded protein was purified using ion exchange chromatography (Q Sepharose), followed by an enterokinase cleavage step and final SEC.

Human KLK7 fluorescence-lifetime assay. Recombinant human KLK7 (5 nM concentration) was pre-incubated with inhibitor at various concentrations for 1 h at room temperature in 50 mM sodium citrate buffer at pH 5.6, containing 150 mM NaCl and 0.05% (w/v) CHAPS. The enzyme reaction was initiated by addition of the substrate Ac-Glu-Phe-Lys-Pro-Ile-Leu-Trp-Arg-Leu-Gly-Cys(PT14)-Glu-NH_2 (0.8 µM; Biosyntan, Berlin, Germany, product BS-#7599). Fluorescence-lifetime measurements were conducted on an Ultra Evolution fluorescence lifetime reader (TECAN, Männedorf, Switzerland). The excitation light source was a semiconductor laser at 405 nm, producing picosecond light pulses with a selected repetition frequency of 10 MHz. The emission was collected through a 450 nm bandpass filter with 25 nm bandwidth. The measurement time per well was set to 1 s, yielding approximately 1,000 counts in the peak channel. The parameters used as assay readout were the mono-exponential lifetimes. IC_{50} values were calculated from the plot of percentage of inhibition vs. inhibitor concentration using nonlinear regression analysis.

Complement FD thioesterolysis assay. The FD thioesterolysis assay was performed according to published procedures[12]. Briefly, recombinant human or murine FD catalytic domain (10 nM concentration) were incubated with compound at various concentrations for 1 h at room temperature in 0.1 M Hepes buffer (pH 7.5) containing 1 mM $MgCl_2$, 1 M NaCl and 0.05% CHAPS. The substrate Z-Lys-thiobenzyl (Bachem, Bubendorf, Switzerland) and 2,4-dinitrobenzenesulfonyl-2,7-desmethyl-fluorecein were added to final concentrations of 200 µM and 25 µM, respectively. The increase in fluorescence was recorded at an excitation wavelength of 485 nm and an emission wavelength of 535 nm in a microplate spectrofluorimeter. IC_{50} values were calculated from percentage of inhibition of FD activity as a function of inhibitor concentration.

Human FD proteolysis assay (ELISA Ba). Recombinant human FD (10 nM concentration) was incubated with compound at various concentrations for 1 h at room temperature in 0.1 M PBS (pH 7.4) containing 7.5 mM $MgCl_2$ and 0.075% (w/v) CHAPS. The preformed CVF–human-FB-substrate complex was added to a final concentration of 200 nM. After 1 h incubation time at room temperature, the enzyme reaction was stopped by addition of a 0.1 M Na_2CO_3 buffer solution (pH 9.0) containing 0.15 M NaCl and 40 mM EDTA. Generation of Ba as the enzymatic cleavage product was quantified by an enzyme-linked-immunosorbent assay (ELISA). Aliquots of reaction samples were pipetted into 384-well high-capacity protein-binding plates (NUNC MaxiSorp) pre-filled with 96 µL/well of coating buffer. After an overnight incubation at 4 °C, assay plates were washed with PBS–Tween 20. Remaining free binding capacity was saturated by the addition of Starting Block T20 for 5 min at room temperature, and assay plates were then washed with PBS–Tween 20. Anti Ba neoepitope antibody was added to each well, followed by incubation for 60 min at room temperature and removal of excess antibody by washing with PBS–Tween 20. Then, goat anti-rabbit antibody labeled with HRP (172-1019; Bio-Rad) (1 µg/well in PBS–Tween 20) was incubated for 60 min at room temperature as in the former step, and excess antibodies was removed by extensive washing with PBS–Tween 20. HRP activity was measured after 20 min incubation time with QuantaBlu fluorogenic peroxidase substrate (100 µL) at room temperature. IC_{50} values were calculated from percentage of inhibition of FD activity as a function of test compound concentration.

Human FB proteolysis assay (ELISA C3a). Human CVF–Bb complex (3 nM concentration) was incubated with compound at various concentrations for 1 h at room temperature in PBS at pH 7.4, containing 10 mM $MgCl_2$ and 0.05% (w/v) CHAPS. The enzyme reaction was started by addition of C3 diluted in the assay buffer to a final concentration of 1 µM. After 1 h incubation time at room temperature, the enzyme reaction was stopped by addition of an excess of various enzyme inhibitors (Roche, cOmplete Inhibitor Tablets). Generation of C3a as the enzymatic cleavage product was quantified by an enzyme-linked immunosorbent assay (ELISA). Aliquots of reaction samples were pipetted into 384-well high-capacity protein-binding plates (NUNC MaxiSorp) pre-filled with 97 µL/well of coating buffer. After an overnight incubation at 4 °C, assay plates were washed with PBS–Tween 20. Remaining free binding capacity was saturated by the addition of Starting Block T20 for 5 min at room temperature, and assay plates were then washed with PBS–Tween 20. Anti-C3a neoepitope antibody was added to each well, followed by incubation for 60 min at room

temperature and removal of excess antibody by washing with PBS–Tween 20. Then, goat anti-mouse antibody labeled with HRP (A0168; Sigma) (0.2 µg/well in PBS–Tween 20) was incubated for 60 min at room temperaure as in the former step, and excess antibody was removed by extensive washing with PBS–Tween 20. HRP activity was measured after 20 min incubation time with Quantablu fluorogenic peroxidase substrate (100 µL) at room temperature. IC_{50} values were calculated from percentage of inhibition of FD activity as a function of test compound concentration.

Membrane-attack complex (MAC) formation assay in 50% human WB. Whole blood (WB) from individual donors was collected under the Novartis employee blood donor program, with informed consent from all participants. Blood was anticoagulated with the thrombin-specific anticoagulant lepirudin (Refludan, Bayer), then diluted in an equal volume of gelatin veronal buffer (GVB; Boston BioProducts) containing 2 mM $MgCl_2$ and 10 mM EGTA (final concentration) for AP activation. Compound serial dilutions were prepared in DMSO, and the 50% WB mixture was pre-incubated with compound for 15 min (final DMSO concentration in all test wells was 0.9%). Zymosan (Sigma) suspension at a final concentration of 1 mg/mL was added to all samples to initiate AP activation, which was allowed to proceed at 37 °C for 40 min. Complement activation was stopped by adding an equal volume of 0.05 M EDTA (final concentration of 25 mM). MAC generation was detected by coating the reaction supernatants onto a 384-well ELISA plate (Nunc Maxisorp). The plate was washed, then incubated with an alkaline phosphatase-conjugated mouse anti-human C9 neoepitope monoclonal antibody (clone aE11, Diatec) at 0.25 µg/mL. After washing, 4-methylumbelliferyl phosphate (4-MUP; Fisher) at 0.18 mg/mL in 0.1 M Tris/HCl (pH 9.0) containing 2 mM $MgCl_2$ was added and the plate was developed for 30 min. The reaction was stopped with an equal volume of 0.2 M EDTA. Plates were read at 355 nm excitation and 460 nm wavelength emission in an appropriate fluorometer. Percentage of inhibition of complement deposition by the compound was calculated relative to the positive control (50% WB with assay buffer) after subtracting the background signal (50% WB with 25 mM EDTA added) to calculate the IC_{50} value using GraphPad Prism software.

Classical and lectin pathway MAC deposition assays. Black MaxiSorp (Life Technologies) plates were coated with human IgM (AbD Serotec) diluted to 10 µg/mL in carbonate buffer (pH 9.5; Sigma) for the classical pathway, or mannan (from *Saccharomyces cerevisiae*; Sigma) diluted to 20 µg/mL in carbonate buffer (pH 9.5) for the lectin pathway assay. Compounds were serially diluted in DMSO in polypropylene V-bottom plates. Normal human serum (Quidel) was diluted to 1% in GVB++ buffer (Boston BioProducts) for the classical, or to 50% in GVB buffer (Boston BioProducts) supplemented to 0.5 mM $MgCl_2$ and 2 mM $CaCl_2$ final concentrations for the lectin pathway assay. Diluted serum was added to the polypropylene plate with compound followed by pre-incubation for 15 min at room temperature and transfer of the mixture to the coated reaction plate. The reaction plate was incubated at 37 °C for 30 min to allow complement activation. The reaction was terminated by washing. MAC formation was detected with an alkaline-phosphatase-conjugated mouse anti-human C9 neoepitope monoclonal antibody (clone aE11, Diatec) at 0.25 µg/mL. After washing, substrate 4-MUP (Fisher) at 0.18 mg/mL in 0.1 M Tris/HCl (pH 9.0) containing 2 mM $MgCl_2$ was added and the plate was incubated for 30 min. Plates were read at 355 nm excitation and 460 nm emission wavelengths on a suitable fluorometer. Percentage inhibition of complement deposition was determined in a similar manner as described above for the 50% human WB assay.

Complement alternate pathway hemolytic assay. Rabbit erythrocytes (Lampire Biological) were washed in cold PBS and resuspended at 8×10^7/mL in GVB buffer (Boston BioProducts) containing 5 mM $MgCl_2$ and 10 mM EGTA. Resuspended erythrocytes (2.5×10^6 cells/well) were combined with 10% (final concentration) normal human serum (Quidel) containing various dilutions of compound in GVB buffer (plus 1% DMSO final concentration) and incubated for 1 h at 37 °C. A 0.1% NP40 (Sigma) solution in GVB was used as the 100% lysis control and GVB containing 1% DMSO was used as the vehicle control in this assay. The reaction mixture was centrifuged and the supernatant was removed to a new plate. Optical density was measured at 415 nm wavelength and percent hemolysis was calculated as: (OD sample – OD vehicle)/(OD 100% lysis – OD vehicle) × 100%.

Mouse C3 cleavage assay. Compound was titrated into serum obtained from wild-type C57Bl/6 or human FD knock-in C57Bl/6 mice and diluted to 50% by addition of gelatin buffer (0.15 mM $CaCl_2$, 141 mM NaCl, 4.5 mM $MgCl_2$, 0.1% gelatin, 20 mM EGTA, 4.2 mM Hepes, pH = 7.3–7.4). Maximal C3 deposition was determined in the absence of compound, and background activity was determined by replacing EGTA with EDTA. After pre-incubation for 30 min at room temperature, 25 uL of serum was added to zymosan-coated plates and incubated for 40 min at room temperature. After washing, C3 deposition was determined by ELISA by using rat anti-mouse C3b/iC3b/C3c antibody in the first step (1 h at 37 °C), followed by HRP-conjugated goat anti-rat IgG (45 min at room temperature) and addition of QuantaBlu (Pierce; #15169). Inhibition was calculated as (OD sample – OD background)/(OD max – OD background) × 100. Data was analyzed using GraphPad Prism, and the IC_{50} value was determined using variable slope (four parameters) curve fitting.

Crystallography. KLK7 in complex with **1** was co-crystallized by the hanging-drop vapor-diffusion method. A volume of 0.5 µL KLK7 solution in the presence of inhibitor **1** (24.6 mg/mL KLK7, 50 mM sodium acetate pH 5.6, 100 mM sodium chloride, 2 mM compound **1**, 1.8% DMSO) was mixed with 0.5 µL reservoir solution (35% PEG 3350, 200 mM $CaCl_2$, 100 mM sodium acetate pH 4.8) and equilibrated against 1 mL reservoir solution. For X-ray data collection, crystals were flash-frozen in liquid nitrogen. X-ray diffraction data were collected from a single crystal at the Swiss Light Source, beamline X10SA, equipped with a MAR 225 CCD detector. The diffraction data were processed and scaled with DENZO and SCALEPACK[36], respectively. The structure was solved by molecular replacement using the program MOLREP[37] and the coordinates of PDB code 1SPJ as a search model.

Human FD was crystallized by the hanging-drop vapor-diffusion method. A 1 µL FD solution (18–18.3 mg/mL FD, 10 mM Tris pH 7.0, 100 mM NaCl) was mixed with 1 µL reservoir solution (22% PEG 3350, 100 mM HEPES pH 7.5 or 25% PEG 3350, 100 mM Tris pH 8.0) and equilibrated against 1 mL reservoir solution. Crystals were soaked by the addition of 0.5 µL inhibitor stock solution (100 mM in 90% DMSO for **4** and **6**, and 10 mM in 90% DMSO for **2**) to the crystal containing drops for 45 min (2 h for compound **6**) and flash-frozen in liquid nitrogen after addition of glycerol as cryoprotectant. X-ray diffraction data were collected from single crystals at the Swiss Light Source, beamline X10SA, equipped with a MAR 225 CCD detector for crystals of FD in complex with **2** and **4**, and a Rigaku FRE rotating anode equipped with a Saturn 92 CCD detector for a crystal of FD in complex with **6**. The diffraction data were processed and scaled with XDS and XSCALE[38], respectively. The structures were solved by molecular replacement using the program MOLREP and the coordinates of PDB code 1BIO as search model. Structures were built using the program COOT[39] and refined using the programs Refmac[40] and BUSTER[41]. Mouse FD was crystallized by the sitting-drop vapor-diffusion method. A 1 µL FD solution (14.4 mg/mL FD, 50 mM Tris pH 8.0, 100 mM NaCl) was mixed with 1 µL reservoir solution (0.1 M HEPES pH 7.0, 30% v/v Jeffamine ED-2001 pH 7.0) and equilibrated against 200 µL reservoir solution. Crystals were cryo-cooled in the reservoir solution with 10% (v/v) added glycerol. All data collection and refinement statistics are summarized in **Supplementary Table 3**. Images were generated using the program PyMOL (http://www.pymol.org)[42].

NMR spectroscopy. A Bruker Avance II 500 MHz and Avance III HD 800 MHz spectrometer equipped with a cryogenically cooled probe head was used. ^1H–^{15}N HSQC were recorded at 310 K using flip-back pulses[43] and a watergate[44,45] sequence for water suppression. The NMR samples contained 100 µM uniformly ^{15}N-labeled FD, 50 mM Tris–D_{11} (Cambridge Isotope Laboratories (CIL), 98% DLM-1814-5), 100 mM NaCl (Fluka catalogue nr. 71376), and 10% D_2O (CIL DLM-2259-1). Compound stock solution was prepared in 90% DMSO-D_6/10% D_2O (v/v) (DMSO-D_6: Eurisotop, St. Aubin Cedex, France, cat. nr. D010ES). The concentration of compounds in buffer was determined by integration of the aromatic ^1H signals and referencing to the internal standard

doi:10.1038/nchembio.2208

DSS (sodium 2,2-dimethyl-2-silapentane-5-sulfonate, CAS (2039-96-5), Cambridge Isotope Laboratories; DLM-32). One-dimensional ^{1}H NMR data were acquired using excitation sculpting for water suppression[46]. Dissociation constants were calculated by assuming the formation of a 1:1 complex and by fitting the chemical shift to the equation:

$$\Delta\delta = \Delta\delta_{\text{bound-free}}((P + L + K_d) - ((P + L + K_d)2 - 4PL)^{0.5})/(2P)$$

Where P is the protein concentration, L is the ligand concentration and $\Delta\delta_{\text{bound-free}}$ is the chemical shift difference between the bound and free protein (in parts per million, p.p.m.). Data fitting was accomplished according to a published protocol (R Core Team. R: A Language and Environment for Statistical Computing. (2014); http://www.r-project.org). Screening of a selected set of small molecules for their potential interaction with latent human FD was conducted by WaterLOGSY at 10 µM protein concentation and 100 µM compound concentration. Spectra were recorded with 256 scans and 1.6 s mixing time at 296 K, and by using excitation sculpting for water suppression[46]. Compounds were screened in mixtures of eight, which results in a total compound concentration of 800 µM per sample. A binding hit was defined by a change-of-sign of the WaterLOGSY signal relative to the unbound compound.

Plasmon resonance (SPR) spectroscopy binding affinity assay. SPR experiments were performed at 25 °C using a Biacore T200 instrument (GE Healthcare). PBS (pH 7.4) supplemented with 0.05% Tween 20 was used as running buffer. Human FD and FB were immobilized covalently to a Series S Sensor Chip CM5 (GE Healthcare) at a flow rate of 10 µL/min using an amine-coupling protocol. Reagents for the immobilization were purchased from GE Healthcare (Amine Coupling Kit; BR-1000-50). The sensor-chip surface was activated by a 5 min injection of a 1:1 (v/v) mixture of a 100 mM *N*-hydroxysuccinimide (NHS) solution and a 390 mM 1-ethyl-3-(3-dimethylaminopropyl)-carbodiimide (EDC) hydrochloride salt solution in water. Both proteins were diluted to 0.05 mg/mL in 20 mM HEPES pH 6.0 for immobilization onto different flow cells of the chip. After a 5 min injection of the protein, remaining reactive groups were deactivated by injecting a 1 M ethanolamine hydrochloride solution in aqueous NaOH (pH 8.5) for 5 min. Different chips were used with immobilization levels ranging between 3,000 and 5,000 response units (RU). To determine kinetic parameters for the binding of compound **6** to human FD and FB, several independent experiments were run. Threefold serial dilutions of compound **6** were prepared ranging from 0.4 to 900 nM. Each solution was injected for 60 s at a flow rate of 30 to 60 µL/min with a dissociation time of at least 1,200 s (parameters identical within one experiment). Two methods were used to determine the kinetic parameters of the interaction: (a) standard kinetics: an independent association–dissociation cycle was run for each concentration by injecting compound solution and waiting for dissociation before the injection of the following concentration, and (b) single cycle kinetics (SCK): five increasing concentrations were injected successively without allowing for the dissociation of the protein–ligand complex. Dissociation of the complex was measured once after the final compound injection. Data was fitted with Biacore T200 Evaluation Software using a Langmuir single-site binding model.

Computational methods: Structure-based library design based on proline center scaffold. The library design concept was based on the prime-site binding pose and key ligand–enzyme interactions observed in the crystal complex of compound **1** bound to human KLK7, and aimed at identifying S1 and S2′ binding motifs more specific for human FD. A virtual library of *N*-urea L-proline-carboxamides was generated from a pool of 3,286 selected commercial amines (MW ≤350; no undesirable functional groups). Compounds were enumerated with Pipeline Pilot (http://accelrys.com/products/collaborative-science/biovia-pipeline-pilot/) and then docked into the adapted 1DIC PDB crystal structure (1.8 Å) of human FD. This modified active site conformation was generated using the Maestro Protein Preparation Wizard (Schrödinger, LLC, New York, NY). All water molecules were removed, the protonation states were set at pH 7.4 using Epik[47], and the imidazole of the catalytic His57 residue was manually protonated (positive charge delocalized). The covalent ligand was removed and the torsional angle for N-Cα-Cβ-OG of the Ser195 side chain was set to $X_1 = 170°$, as observed in the KLK7–inhibitor **1** crystal complex, to allow for direct hydrogen bond interaction of the urea carbonyl of the proline ligand with the NH of Gly193 (referred to as the 'oxyanion hole'; **Fig. 1b**). Ligand docking and scoring was performed with GLIDE by defining the formation of at least one hydrogen bond interaction of ligands in their docking pose, either with the NH of Gly193 and/or the carbonyl of Leu41, as a constraint. Visual inspection of the top-scoring compounds led to the selection of 12 structural motifs filling the S1 pocket and 4 residues suitably positioned in the S2′ pocket of FD. A total of 20 proline-based analogs (out of 48 possible combinations) were synthesized using a similar synthesis protocol as described for compound **2**, followed by compound testing in the FD thioesterolysis assay.

Computational methods: Generation of a focused fragment library for NMR screening by WaterLOGSY. A set of some 52,000 fragments was assembled from the Novartis compound collection by applying a set of filter criteria for molecular properties including molecular weight, number of hydrogen bond acceptor/donor groups and rotatable bond (**Supplementary Fig. 2**). Compounds were docked using GLIDE into the ligand-free active site conformation of FD, which was adapted from the 1DIC PDB crystal structure as described above, and in which Asp189 forms a salt bridge with Arg218 at the bottom of the S1 pocket. Furthermore, a computational model of a more-open FD active site S1 conformation was constructed manually by accounting for FD to specifically recognize an arginine residue at the P1 cleavage site of the FB substrate. The Arg218 side chain was manually displaced from its crystallographic location and was moved to an outward position, allowing the Asp189 to make direct contact with fragments that were potentially binding into the S1 pocket. The same fragment library was then docked with GLIDE into the open protein conformation. The top-scored fragments identified from the two independent docking experiments were visually inspected, clustered according to the type of interactions with the protein (for example, ionic charge–charge, hydrogen bonding, dipole–dipole, others), and representatives from each cluster were finally selected (225 fragments in total) for NMR screening by WaterLOGSY.

Generation of humanized complement FD knock-in mice (B6–Cfd$^{tm1.1(CFD)Npa}$ mice). The mouse *Cfd* genomic sequence containing the promoter, exon 1, intron 1, and 5 nucleotides from exon 2 was amplified by polymerase chain reaction (PCR) from C57Bl/6 mouse genomic DNA (Ensembl gene ID ENSMUSG00000061780) and was fused to the human *CFD* cDNA followed by the mouse *Cfd* 3′ UTR containing a stop codon as well as a poly-adenylation signal. The resulting mouse–human chimeric fragment was subcloned into the vector pRAY-2 containing a floxed neomycin resistance cassette (GenBank accession number U63120) followed by subsequent cloning of a PCR-amplified 3′ homology fragment downstream of neomycin, resulting in the complement FD targeting vector. C57Bl/6 mouse embryonic stem (ES) cells were transfected by electroporation of ScaI-linearized FD targeting vector. Transfected ES cells were selected for neomycin resistance using 0.2 mg/ml geneticin (Invitrogen; #10131-019). Ten days after transfection, 300 G418-resistant ES cell clones were isolated and genotyped by PCR for homologous recombination with the primers CTATCGCCTTCTTGACGA and CCACCAGCCTGCGTATGT. Homologous recombination was confirmed by Southern blot and a positive targeted C57Bl/6 ES cell clone was used for injection into BALB/C host blastocysts, which were then transferred into pseudopregnant CB6F1 foster females. Chimeric males were crossed with C57Bl/6 females and black offspring were genotyped. Removal of the floxed neomycin resistance cassette was done by crossing the mice with a Cre-recombinase-expressing line[48,49] and resulted in mouse strain B6–Cfd$^{tm1.1(CFD)Npa}$, named according to the International Committee on Standardized Genetic Nomenclature for Mice. Primers used for the genotyping of the humanized FD mice were CCTACCCTCCTCAGCAGCAC and CCAGGAGAACCTGCACCTTC.

Surrogate PNH human erythrocyte assay. Serum and heparinized blood from healthy volunteers were provided under informed consent and collected through the Novartis Tissue Donor Program (TRI0128) in accordance with the Swiss Human Research Act and with approval of the responsible ethic committee (Ethikkommission Nordwest- und Zentralschweiz). Serum was prepared by addition of Mg^{2+}–EGTA (8 mM EGTA and 2.85 mM $MgCl_2$ final concentration) to prevent antibody-mediated activation of the classical complement pathway,

and acidified to pH 6.4 by addition of aqueous HCl solution. Serial dilutions of compound **6**, **7**, or anti-C5 eculizumab were prepared directly in acidified serum and were incubated on ice for 10 min. In parallel, to mimic a PNH-like phenotype, red blood cells (RBCs) from the same donor were masked by addition of 10 µg/mL anti-CD55 and 30 µg/mL anti-CD59 for 30 min at 37 °C with agitation (2×10^9 cells/mL) in HEPES-containing GVBreplacement (GVBR) (0.15 mM $CaCl_2$, 145 mM NaCl, 0.1% gelatin, 4.2 mM HEPES, 5.7 mM $MgCl_2$, pH 7.5). After washing in PIPES-containing GVBR (0.15 mM $CaCl_2$, 145 mM NaCl, 0.1% gelatin, 10 mM PIPES, 5.7 mM $MgCl_2$, pH 6.4), 2×10^7 masked RBCs per well were plated in a 96-deep-well plate containing 240 µL/well acidified serum. Erythrocytes were incubated in pure water or in 10 mM EDTA solution as controls (for maximal lysis and minimal lysis, respectively). The plate was sealed with a plastic adhesive film and incubated for 1 h at 37 °C with agitation. To terminate the reaction, 200 µL/well of GVBR containing 15 mM EDTA was added and the plate was centrifuged at 4,000 r.p.m. for 5 min. Then, 100 µL of the supernatant was transferred into a 96-well microplate and the absorbance at 405 nm wavelength was measured using a SpectraMax 340PC Microplate Reader. The relative percentage of hemolysis was determined using the absorbance in EDTA-treated serum (negative control) as baseline (i.e., 0% hemolysis) and the absorbance measured with the positive control (water) as maximim (100% hemolysis). Averages of the control quadruplets were calculated.

$$\%\,\text{hemolysis} = \frac{(\text{sample value} - \text{average baseline}) * 100}{\text{average maximum}}$$

For fluorescence-activated cell sorting (FACS) analysis of complement fragments, red blood cells and supernatant of the incubated 96-deep-well plate were transferred into 1.5 mL Eppendorf tubes and washed with FACS buffer. All centrifugation steps were carried out at 11,000 r.p.m. for 5 to 7 min at 4 °C. The antibodies anti-C3d(neo) and anti-C5b-9 were labeled with Zenon Labeling Kits following the manufacturer's protocol. RBCs were incubated with Zenon-labeled antibodies (0.5 µg per stain) for 30 min at 4 °C in the dark. After staining, RBCs were washed with FACS buffer and filtered before FACS acquisition. Analysis was performed with an LSRFortessa Cell Analyzer (BD Biosciences).

IC_{50} values were calculated with GraphPad Prism using the equation: log(inhibitor) vs. response – variable slope (four parameters). The reported IC_{50} is an average of a total of 11, 2, and 7 experiments performed in duplicate for compounds **6**, **7**, and eculizumab, respectively. The FACS data was analyzed with the software FlowJo X. The debris was always gated out as much as possible.

***Ex vivo* PNH patient erythrocyte assay.** Peripheral blood was collected from healthy volunteers (as a source for ABO-matched normal sera) and from PNH patients. For consistency, blood was serially drawn from the same three untreated patients, who exhibited a large PNH cell population (>10% on erythrocytes, >50% on granulocytes) for all experiments. Blood was collected in standard EDTA and serum Vacutainer tubes (BD Pharmingen) after venipuncture according to standard procedures and following informed consent as approved by the local IRB. This study was conducted in accordance with the Declaration of Helsinki. Erythrocytes were obtained from peripheral blood after three washings in saline and were subsequently incubated with Mg^{2+}-supplemented sera from ABO-matched healthy individuals (NHS) at final hematocrits of 2%. In order to reduce inter-experiment variability, pooled sera from at least three subjects all with plasma C3 in the normal range were used. AP activation was achieved by acidification using HCl (1:20 of 0.1 N HCl), which resulted in a pH drop to a value between 6.7 and 6.9. Compound was added to the tubes at different concentrations before complement activation. After 24 h incubation time at 37 °C in acidified NHS (AcNHS), hemolysis was quantified by flow cytometry after staining of the erythrocyte pellet with a FITC-conjugated anti-C3 polyclonal antibody (Ab14396; Abcam) and a PE-conjugated anti-CD59 monoclonal antibody (59-PE; Valter Occhiena). In brief, hemolysis was measured by comparing baseline (pre) and post-incubation (post) percentage of PNH RBCs. The proportion of surviving PNH RBCs (% PNH post/% PNH pre) was normalized, based on the determination of residual normal RBCs (dividing by % N post/% N pre). The rate of hemolysis was then calculated as the reciprocal of the percentage of survival. This finally leads to the formula previously published by Ferreira *et al.*[50]: % lysis = 100 – (% PNH post/% N post) × (% N pre/% PNH pre) × 100.

The same anti-C3 and anti-CD59 staining also served to assess opsonization by evaluating the deposition of C3 fragments on erythrocytes exposed to AP activation in the presence of compound **7** using flow cytometry at the end of the hemolytic assay. The anti-C3 used in this study (Ab14396) has been shown to bind both C3b and its degradation fragments iC3b and C3dg[49]. Inhibition in the presence of 1 µM compound **7** was calculated by determining the average percent hemolysis of PNH erythrocytes at the indicated conditions for three individual patients (2 to 14 experiments were performed per patient). Finally, the individual mean result for each patient was averaged and s.e.m. was calculated with GraphPad Prism and significance was determined using one-way analysis of variance (ANOVA) followed by Tukey's multiple comparison test.

***In vivo* studies: Animals and LPS-induced complement activation.** B6–$Cfd^{tm1.1(CFD)Npa}$ mice or wild type C57Bl/6 mice were maintained at Taconic Farms (Germantown NY, USA) and female 6-week old animals were brought in-house for experiments. Mice were housed in a pathogen-free facility on a 12 h light/dark cycle. Mice were fed with standard rodent laboratory chow and sterile water ad libitum. Protocols, handling and care of the mice were in accordance with the policy of the NIBR Cambridge Animal Care and Use Committee. Studies were performed in 7-week-old mice weighing approximately 20 g. Complement activity was induced by intraperitoneal injection of 50 µg of lipopolysaccharide (LPS) from *Salmonella* typhimurium (Sigma) dissolved in 100 µL sterile PBS per animal. In these studies, negative-control animals received an intraperitoneal injection of 100 µL sterile normal saline solution, and dosing vehicle alone (consisting of the formulations detailed below, minus the drug) by oral gavage. Positive control animals received intraperitoneal LPS and dosing vehicle alone by oral gavage. For compound administration, either a solution formulation in 20% propylene glycol and 10% solutol in water, or a suspension formulation using 0.5% methylcellulose and 0.5% Tween 80 in water, was prepared. For dose–response studies, LPS (or PBS) was administered 7.5 h before end of study (time = 0), and compound at various doses (or vehicle) was administered by oral gavage 3.5 h later, or 4 h before the end of the study. For duration of action studies, groups of mice (grouped per time point) were given one dose of compound by oral gavage at 24, 16, 10, 8, 6, or 4 h before the end of the study (time = 0). All groups were given LPS by intraperitoneal injection 7.5 h before the end of the study. See **Supplementary Figure 5** for a schematic depiction of the study designs.

Tissue collection and preparation of eye extracts. Mice were euthanized at indicated times. Plasma was collected in microtainer EDTA tubes (Becton Dickinson). Eyes without lens were collected in 2 mL microcentrifuge tubes (Fisher), frozen quickly on dry ice, and stored at −80 °C. Eye extracts were prepared by adding 200 µL of cell-lysis buffer consisting of 1× cell lysis buffer (Cell Signaling Technology), 1× complement mini protease inhibitor cocktail EDTA-free tablet (Roche Diagnostics), 1 mM PMSF (Sigma) and 20 mM PNPP to each sample tube. Eye tissues were then lysed with TissueLyser II (Qiagen) and tissue debris was pelleted by centrifugation at 11,000 r.p.m. at 4 °C for 10 min. Supernatants were transferred to either a new tube or a 96-well plate and stored at −80 °C. The Bradford assay (Bradford M 1976; Pierce) was used to determine the protein concentration of the respective samples.

Protein gel and western blot analysis. Equal amounts of either eye protein extract (~40 µg protein) or 0.5 µL sampled plasma was resolved electrophoretically on denaturing SDS polyacrylamide gels (NuPAGE 4–12% Bis–Tris gel; NOVEX/Invitrogen), then transferred onto nitrocellulose membranes (iBlot Gel Transfer Stacks Nitrocellulose; NOVEX/Invitrogen) by semi-dry blotting (iBlot) for 7 min. The nitrocellulose membrane was incubated with blocking buffer (Odyssey) for 30 min and probed overnight at 4 °C with either goat polyclonal anti-mouse C3d (AF2655; R & D Systems) or anti-factor B (A311; Quidel) primary antibody diluted by 1:2,000 in blocking buffer. The first antibody recognized any mouse-C3d-containing proteins, including the full-length C3 alpha chain (120 kDa), the C3 cleavage fragments C3b, iC3b (68 kDa), and C3d (41 kDa). Blots were washed three times with TBST by changing the buffer every 10 min and then were incubated for 1 h at room temperature with

doi:10.1038/nchembio.2208

the infrared fluorescently conjugated IRDye 800CW donkey anti-goat IgG (605-731-125; Rockland) secondary antibody diluted by 1:5,000 in blocking buffer. Blots were washed again as described above and infrared fluorescent signals were detected with an Odyssey imager (LI-COR). Fluorescent signals were directly proportional to the amount of the antigen on Odyssey western blots. The average fluorescent intensity in C3d (41 kDa) and iC3b (68 kDa) bands, or the Ba (33 kDa) band, assigned based on their positions relative to protein molecular weight markers (Bio-RAD), were quantified using Odyssey software.

Plasma samples (0.5 µL each) from human FD knock-in mice (B6–Cfd$^{tm1.1(CFD)Npa}$ mice) were resolved on SDS gels and transferred to nitrocellulose membranes. A serially diluted recombinant human FD protein (preparation described above) was loaded in the same gel to serve as the standard. The membranes were blocked using the Odyssey blocking buffer (Li-Cor) and were incubated with an anti-FD (AF1824; R&D) antibody overnight at 4 °C. An infrared fluorescently conjugated IRDye 800CW donkey anti-goat IgG (605-731-125; Rockland) was used as the secondary antibody to visualize the expected human FD protein band (~25 kDa). The fluorescent intensity of the FD protein was captured using Odyssey imager and software (Li-Cor). Serum FD concentration in each animal was extrapolated from the standard curve using Prism (GraphPad) software.

Statistical methods and *in vivo* data analyses. Data are presented as group mean ± s.e.m. Groups consisted of 4 to 10 mice as indicated. Mean differences were compared and considered statistically significant when $P < 0.05$ measured by one-way analysis of variance, followed by correction for multiple comparisons using Dunnett's post-test, where $^{*}P < 0.05$, $^{**}P < 0.01$, $^{***}P < 0.001$ compared to the LPS + vehicle-treated positive control group. Data was analyzed by subtracting the baseline values of Ba or C3d+iC3b levels measured in the PBS+vehicle treated groups from the respective values for each LPS treated group. Using the baseline-subtracted values, the percent inhibition was calculated as: % inhibition = (1 – (value of Ba or C3d+iC3b in presence of LPS and compound) / average value of Ba or C3d+iC3b in LPS + vehicle group) × 100. Each type of *in vivo* experiment (dose–response or duration of action study) was conducted at least twice. Using liquid chromatography coupled to mass spectrometry (LC–MS), plasma levels of **6** were determined in individual samples at the terminal time point from both dose–response and duration of action studies. These exposure data were used, in conjunction with the individual plasma Ba inhibition results, to determine the *in vivo* half-maximal efficacious concentration (EC_{50}) for **6** using nonlinear regression curve fitting with GraphPad Prism.

Pharmacokinetic studies. The pharmacokinetics of compound **7** were determined in 6–10 week old male Sprague Dawley rats ($n = 2$) following a single intravenous (i.v.) (1 mg per kg body weight) and a single peroral (p.o.) (1 mg per kg body weight) dose, respectively. The i.v. formulation was prepared as a 1.0 mg/mL solution containing 5% EtOH, 10% PG, 25% of a 20% solutol solution, and water for injection and animals were dosed by injection into the cannula of the jugular vein. The same vehicle was used for the preparation of a 0.1 mg/mL solution of compound which was administered by oral gavage (10 mL per animal). Approximately 50 µL of whole blood was collected from the tail at 5 min (i.v. dose only), 15 min (p.o. only), 0.5, 1, 2, 4, 7, and 24 h post-dose and transferred to a EDTA tubes. Blood was centrifuged at 3,000 r.p.m. and the resultant plasma was transferred to a PCR 96-well plate, capped with PCR strip cap and stored frozen (–20 °C) for parent compound analysis.

High performance liquid chromatography (HPLC)-MS/MS methods were developed and used to quantify compound in plasma. Aliquots (25 µL) of plasma from the *in vivo* samples and from calibration standards were de-proteinated by adding acetonitrile (150 µL) containing 50 ng/mL of an internal standard (glyburide), followed by vortexing for 10 min and centrifugation for 5 min at 4,000 r.p.m. (2,800 g) at 4 °C. For HPLC–MS/MS analyses using a MAC-MOD ACE C18 column (Mac-Mod Analytical), the supernatant (125 µL) of each well was transferred to a new plate and diluted by addition of 50 µL of water. Pharmacokinetic parameters, including the area under the curve (AUC), were calculated using the linear trapezoidal rule. Extrapolated initial concentration (C_0), maximal concentration (C_{max}), volume of distribution (V_{ss}), clearance (CL) and terminal half-life ($T_{1/2}$), were estimated using non-compartmental methods using WinNonlin (Enterprise, Version 5.2) purchased from Pharsight Corporation (St. Louis, MO).

34. Maeda, H. *et al.* 2,4-Dinitrobenzenesulfonyl fluoresceins as fluorescent alternatives to Ellman's reagent in thiol-quantification enzyme assays. *Angew. Chem. Int. Ed. Engl.* **44**, 2922–2925 (2005).
35. Harris, C.L., Lublin, D.M. & Morgan, B.P. Efficient generation of monoclonal antibodies for specific protein domains using recombinant immunoglobulin fusion proteins: pitfalls and solutions. *J. Immunol. Methods* **268**, 245–258 (2002).
36. Otwinowski, Z. & Minor, W. Processing of X-ray diffraction data collected in oscillation mode. *Methods Enzymol.* **276**, 307–326 (1997).
37. Vagin, A. & Teplyakov, A. MOLREP: an automated program for molecular replacement. *J. Appl. Cryst.* **30**, 1022–1025 (1997).
38. Kabsch, W. Automatic processing of rotation diffraction data from crystals of initially unknown symmetry and cell constants. *J. Appl. Cryst.* **26**, 795–800 (1993).
39. Emsley, P., Lohkamp, B., Scott, W.G. & Cowtan, K. Features and development of Coot. *Acta Crystallogr. D Biol. Crystallogr.* **66**, 486–501 (2010).
40. Murshudov, G.N., Vagin, A.A. & Dodson, E.J. Refinement of macromolecular structures by the maximum-likelihood method. *Acta Crystallogr. D Biol. Crystallogr.* **53**, 240–255 (1997).
41. Blanc, E. *et al.* Refinement of severely incomplete structures with maximum likelihood in BUSTER-TNT. *Acta Crystallogr. D Biol. Crystallogr.* **60**, 2210–2221 (2004).
42. The PyMOL Molecular Graphics System V.1.7.6.5. (Schrödinger, LLC, 2002).
43. Mori, S., Abeygunawardana, C., Johnson, M.O. & van Zijl, P.C.M. Improved sensitivity of HSQC spectra of exchanging protons at short interscan delays using a new fast HSQC (FHSQC) detection scheme that avoids water saturation. *J. Magn. Reson. B.* **108**, 94–98 (1995).
44. Piotto, M., Saudek, V. & Sklenár, V. Gradient-tailored excitation for single-quantum NMR spectroscopy of aqueous solutions. *J. Biomol. NMR* **2**, 661–665 (1992).
45. Sklenar, V., Piotto, M., Leppik, R. & Saudek, V. Gradient-tailored water suppression for $^{1}H–^{15}N$ HSQC experiments optimized to retain full sensitivity. *J. Magn. Reson. A* **102**, 241–245 (1993).
46. Hwang, T.L. & Shaka, A.J. Water suppression that works. Excitation sculpting using arbitrary waveforms and pulsed field gradients. *J. Magn. Reson. A* **112**, 275–279 (1995).
47. Shelley, J.C. *et al.* Epik: a software program for pK(a) prediction and protonation state generation for drug-like molecules. *J. Comput. Aided Mol. Des.* **21**, 681–691 (2007).
48. Schwenk, F., Baron, U. & Rajewsky, K. A *cre*-transgenic mouse strain for the ubiquitous deletion of *loxP*-flanked gene segments including deletion in germ cells. *Nucleic Acids Res.* **23**, 5080–5081 (1995).
49. Jägle, U., Gasser, J.A., Müller, M. & Kinzel, B. Conditional transgene expression mediated by the mouse β-actin locus. *Genesis* **45**, 659–666 (2007).
50. Ferreira, V.P. & Pangburn, M.K. Factor H mediated cell surface protection from complement is critical for the survival of PNH erythrocytes. *Blood* **110**, 2190–2192 (2007).